high imperfection. (In reflection topographs, imperfect regions will always produce stronger *integrated* reflections than perfect regions and will also do so in transmission topographs under low-absorption conditions.) The island $B$ is assumed to be as perfect as $C$, but is slightly misoriented with respect to $C$. The topograph images sketched in ($b$)–($e$) could represent either reflection topographs or transmission topographs from a specimen thin compared with the dimension $CD$ in Fig. 2.7.1.2. [Possible distortion of the images relative to the shape of ($a$) is neglected: this matter is considered later.] First, suppose that continuous radiation is emitted from the source $S$. If the ratio $b/a$ is quite small, the topograph image will resemble ($b$). The island $A$ is detected by diffraction contrast whereas island $B$ will not show any area contrast since by assumption the incident radiation contains wavelengths enabling $B$ to satisfy the Bragg condition just as well as $C$. The low-angle $B$–$C$ boundary may show up, however, since it contains dislocations that will produce diffraction contrast and might be individually resolvable with a high-resolution topographic technique. Orientation contrast of $B$ becomes manifest when $b$ is increased, and measurement of the misorientation is then possible from the displacement of the image of $B$ [as shown in ($c$)] consequent upon the different direction of Bragg-reflected rays issuing from it compared with those from $C$.

Next, suppose that $S$ emits a limited range of wavelengths, *e.g.* characteristic $K\alpha$ radiation, and let the incident beam be collimated to have an angular spread in the plane of incidence that is smaller than the component in that plane of the misorientation between $B$ and $C$, but larger than the angular range of reflection of $C$ or $A$. Then, if the specimen is rotated about the $\omega$ axis so that $A$ and $C$ satisfy the Bragg condition, $B$ will not do so and the topograph will resemble ($d$). [Island $A$ shows up in ($d$) by diffraction contrast, as in ($b$).]. Appropriate rotation of the specimen will bring $B$ into the Bragg-reflecting orientation, but will eliminate reflection from $A$ and $C$, as shown in ($e$). The images ($d$) and ($e$) will not undergo significant change with variation in the ratio $b/a$, except for loss of resolution as $b/a$ increases. The sensitivity of misorientation measurement will increase as the angular and wavelength spread of the incident beam are reduced, but when the angular range of a monochromatic incident beam is lowered to a value comparable with the angular range of reflection of the perfect crystal (generally only a few seconds of arc), it will not be possible with one angular setting alone to obtain an image that will distinguish between diffraction contrast and orientation contrast in the clear way shown in ($d$). The distinction will require comparison of a series of topographs obtained during a step-wise sweep of the angular range of reflection by the specimen. This is the procedure adopted in double-crystal or multicrystal topography, as described in Sections 2.7.3 and Subsection 2.7.4.2.

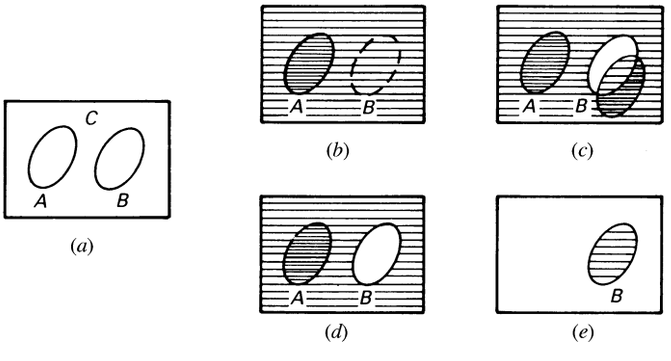


Fig. 2.7.1.3. Differentiation between orientation contrast and diffraction contrast in types of topograph images, ($b$)–($e$), of a crystal surface ($a$).

Details concerning diverse variants in diffraction geometry used in X-ray topographic experiments, treatments of the diffraction contrast theory underlying X-ray topographic imaging of lattice defects, and listings of applications of X-ray topography can be found in reviews and monographs of which a selection follows. All aspects of X-ray topography are covered in the survey edited by Tanner & Bowen (1980). Armstrong & Wu (1973), Tanner (1976), and Lang (1978) describe experimental techniques and review their applications. The dynamical-diffraction theoretical basis of X-ray topography is emphasized by Authier (1970, 1977). Kato (1974) and Pinsker (1978) deal comprehensively with X-ray dynamical diffraction theory, which is also the topic of Part 5 of *IT* B (1996). Introductions to this theory have been presented by Batterman & Cole (1964), Hart (1971), and Hildebrandt (1982), the latter two being especially relevant to X-ray topography.

## 2.7.2. Single-crystal techniques

### 2.7.2.1. *Reflection topographs*

Combining the simple diffraction geometry of Fig. 2.7.1.1 with a laboratory microfocus source of continuous radiation offers a simple yet sensitive technique for mapping misorientation textures of large single crystals (Schulz, 1954). One laboratory X-ray source much used produces an apparent size of $S$ 30 μm in the axial direction and 3 μm in the plane of incidence. Smaller source sizes can be achieved with X-ray tubes employing magnetic focusing of the electron beam. Then $b/a$ ratios between $\frac{1}{2}$ and 1 can be adopted without serious loss of geometric resolution, and, with $a = 0.3$ m typically, misorientation angles of $10''$ can be measured on images of the type ($c$) in Fig. 2.7.1.3. The technique is most informative when the crystal is divided into well defined subgrains separated by low-angle boundaries, as is often the case with annealed melt-grown crystals. On the other hand, when continuous lattice curvature is present, as is usually the case in all but the simplest cases of plastic deformation, it is difficult to separate the relative contributions of orientation contrast and diffraction contrast on topographs taken by this method. In principle, the separation could be effected by recording a series of exposures with a wide range of values of $b$, and it becomes practicable to do so when exposures can be brief, as they can be with synchrotron-radiation sources (see Section 2.7.4.).

For easier separation of orientation contrast and diffraction contrast, and for quicker exposures with conventional X-ray sources, collimated characteristic radiation is used, as in the Berg–Barrett method. Barrett (1945) improved an arrangement earlier described by Berg (1931) by using fine-grain photographic emulsion and by minimizing the ratio $b/a$, and achieved high topographic resolution (~ 1 μm). The method was further developed by Newkirk (1958, 1959). A typical Berg–Barrett arrangement is sketched in Fig. 2.7.2.1. Usually, the source $S$ is

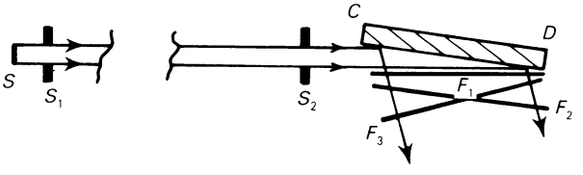


Fig. 2.7.2.1. Berg–Barrett arrangement for surface-reflection topographs.

the focal spot of a standard X-ray tube, giving an apparent source 1 mm square perpendicular to the incident beam. The openings of the slits $S_1$ and $S_2$ are also 1 mm in the plane of incidence, and the distance $S_1$–$S_2$ (which may be identified with the distance $a$) is typically 0.3 m. The specimen is oriented so as to Bragg reflect asymmetrically, as shown. Softer radiations, *e.g.* Cu $K\alpha$, Co $K\alpha$ or Cr $K\alpha$, are employed and higher-angle Bragg reflections are chosen ($2\theta_B \simeq 90^\circ$ is most convenient). Fig. 2.7.2.1 indicates three possible film orientations, $F_1$–$F_3$. (These possibilities apply in most X-ray topographic arrangements.) Choice of orientation is made from the following considerations. If minimum distance $b$ is required over the whole length $CD$, then position $F_1$ is most appropriate. If a geometrically undistorted image of $CD$ is needed, then position $F_2$, in which the film plane is parallel to the specimen surface, satisfies this condition. If a thick emulsion is used, it should receive X-rays at normal incidence, and be in orientation $F_3$. If high-resolution spectroscopic photographic plates are used, in which the emulsion thickness is $\sim 1\,\mu$m only, then considerable obliquity of incidence of the X-rays is tolerable. But these plates have low X-ray absorption efficiency. Nuclear emulsions (particularly Ilford type L4) are much used in X-ray topographic work. Ilford L4 is a high-density emulsion (halide weight fraction 83%) and hence has high X-ray stopping power. The usual minimum emulsion thickness is 25 μm. Such emulsions should be oriented not more than about 2° off perpendicularity to the X-ray beam if resolution loss due to oblique incidence is not to exceed 1 μm (with correspondingly closer limits on obliquity for thicker emulsions). With 1 mm openings of $S_1$ and $S_2$, and $a = 0.3$ m, most of the irradiated area of $CD$ will receive an angular range of illumination sufficient to allow both components of the $K\alpha$ doublet to Bragg reflect. In these circumstances, the distance $b$ must be everywhere less than 1–2 mm if image spreading due to superimposition of the $\alpha_1$ and $\alpha_2$ images is not to exceed a few micrometres. In order to eliminate this major cause of resolution loss (and, incidentally, gain sensitivity in misorientation measurements), the apertures $S_1$ and $S_2$ should be narrowed and/or $a$ increased so that the angular range of incidence on the specimen is less than the difference in Bragg angle of the $\alpha_1$ and $\alpha_2$ components for the particular radiation and Bragg angle being used. (This condition applies equally in the transmission specimen techniques, described below.). With a narrower beam, the illuminated length of $CD$ is reduced. This disadvantage may be overcome by mounting the specimen and film together on a linear traverse mechanism so that during the exposure all the length of $CD$ of interest is scanned. In this way, surface-reflection X-ray topographs can be recorded for comparison with, say, etch patterns or cathodoluminescence patterns (Lang, 1974).

### 2.7.2.2. *Transmission topographs*

The term 'X-ray topograph' was introduced by Ramachandran (1944) who took transmission topographs of cleavage plates of diamond using essentially the arrangement shown in Fig. 2.7.1.2. (In this case, $S$ was a 0.3 mm diameter pinhole placed in front of the window of a W-target X-ray tube so as to form a point source of diverging continuous radiation.) Ramachandran adopted a distance $a = 0.3$ m and ratio $a/b$ of about 12, which produced images of about 25 μm geometrical resolution having the characteristics of Fig. 2.7.1.3(*b*), *i.e.* sensitive to diffraction contrast but not to orientation contrast. For each reflection under study, the film was inclined to the incident beam with that obliquity calculated to produce an undistorted image of the specimen plate. Guinier & Tennevin (1949) studied both diffraction contrast and orientation contrast in continuous-radiation transmission topograph images. Their minimum $b/a$ ratio was set by the need to avoid overlap of Laue images of the crystal produced by different Bragg planes.

Collimated characteristic radiation is used in the methods of 'section topographs' (Lang, 1957) and 'projection topographs' (Lang, 1959*a*), the latter being sometimes called 'traverse topographs'. Fig. 2.7.2.2 explains both techniques. When taking a section topograph, the specimen $CD$, usually plate shaped, is stationary (disregard the double-headed arrow in the figure). The ribbon-shaped incident beam issuing from the slit $P$ is Bragg reflected by planes normal, or not far from normal, to the major surfaces of the specimen. As drawn, the Bragg planes make an angle $\alpha$ with the normal to the X-ray entrance surface of the specimen, the positive sense of $\alpha$ being taken in the same sense as the deviation $2\theta_B$ of the Bragg-reflected rays. If the crystal is sufficiently perfect for multiple scattering to occur within it (with or without loss of coherence), then the multiply scattered rays associated with the Bragg reflection excited will fill the volume of the triangular prism whose base is $ORT$, the 'energy-flow triangle' or 'Borrmann triangle', contained between $OT$ and $OR$ whose directions are parallel to the incident wavevector, $\mathbf{K}_0$, and diffracted wavevector, $\mathbf{K}_h$, respectively. Both the $\mathbf{K}_0$ and $\mathbf{K}_h$ beams issuing from the X-ray exit surface of the crystal carry information about the lattice defects within the crystal. However, it is usual to record only the $\mathbf{K}_h$ beam. This falls on the film, $F$, in a strip extending normal to the plane of incidence, of height equal to the illuminated height of the specimen multiplied by the axial magnification factor $(a + b)/a$, and forms the section topograph image. The screen, $Q$, prevents the $\mathbf{K}_0$ beam from blackening the film but has a slot allowing the diffracted beam to fall on $F$. A diffraction-contrast-producing lattice defect cut by $OT$ at $I$ will generate supplementary rays parallel to $\mathbf{K}_h$ and will produce an identifiable image on $F$ at $I'$, the 'direct image' or 'kinematic image' of the defect. The depth of $I$ within $CD$ can be found *via* the measurement of $I'T'/R'T'$. From a series of section topographs taken with a known translation of the specimen between each topograph, a three-dimensional construction of the trajectory of defect $I$ (*e.g.* a dislocation line) within the crystal can be built up. To obtain good definition of the spatial width of the ribbon incident beam cutting the crystal, the distance between $P$ and the crystal is kept small. The minimum practicable opening of $P$ is about 10 μm. If diffraction is occurring from planes perpendicular to the X-ray entrance surface of the specimen, *i.e. symmetrical Laue case* diffraction, the width $R'T'$ of the section topograph image is simply $2t \sin\theta_B$, $t$ being the specimen thickness, and neglecting the contribution from the

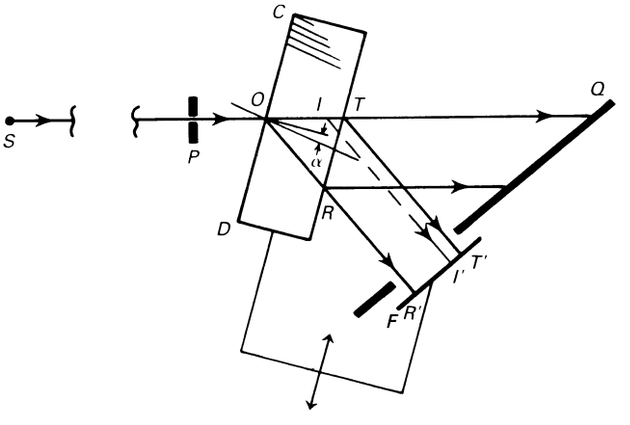


Fig. 2.7.2.2. Arrangements for section topographs and projection topographs.

width of the ribbon incident beam. With asymmetric transmission, as drawn in the figure, $R'T' = t\sec(\theta_B - \alpha)\sin 2\theta_B$. The distance $b$ is made as small as is permitted by the specimen shape and the need to separate the emerging $\mathbf{K}_0$ and $\mathbf{K}_h$ beams. Suppose $b$ is 10 mm. Then, with a source $S$ having axial extension 100 μm, the distance $a = SP$ should be not less than 0.5 m in order to keep the geometrical resolution in the axial direction better than 2 μm, and should be correspondingly longer with larger source sizes.

To take a projection topograph, the specimen $CD$ and the cassette holding the film $F$ are together mounted on an accurate linear traversing mechanism that oscillates back and forth during the exposure so that the whole area of interest in the specimen is scanned by the ribbon beam from $P$. The screen $Q$ is stationary. If the specimen is plate shaped, the best traverse direction to choose is that parallel to the plate, as indicated by the double-headed arrow, for then the diffracted beam will have minimum side-to-side oscillation during the traverse oscillation, the opening of $Q$ can be held to a minimum, and thereby unwanted scattering reaching $F$ kept low. The projection topograph image is an orthographic projection parallel to $\mathbf{K}_h$ of the crystal volume and its content of diffraction-contrast-producing lattice defects. If the specimen is plate-like, of length $L$ in the plane of incidence, then, with $F$ normal to $\mathbf{K}_h$, the magnification of the topograph image in the direction parallel to the plane of incidence is $L\cos(\theta_B + \alpha)$. There will generally be a small change of axial magnification $(a + b)/a$ along $L$. The loss of three-dimensional information occurring through projection can be recovered by taking stereopairs of projection topographs. The first method (Lang, 1959*a*,*b*) used $hkl$, $\bar{h}\bar{k}\bar{l}$ pairs of topographs as stereopairs. One disadvantage of this method is that the convergence angle is fixed at $2\theta_B$, which may be unsuitably large for thick specimens. The method of Haruta (1965) obtains two views of the specimen using the same $hkl$ reflection, by making a small rotation of the specimen about the **h** vector between the two exposures, and has the advantage that this rotation, and hence the stereoscopic sensitivity, can be chosen at will. When taking projection topographs, the slit $P$ can be wider than the narrow opening needed for high-resolution section topographs, but not so wide as to cause unwanted $K\alpha_2$ reflection to occur. Best use of the X-ray source is made when the width of $P$ is the same as or somewhat greater than $S$.

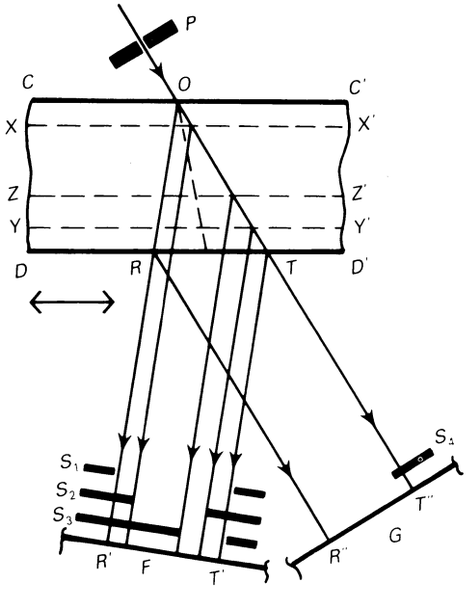


Fig. 2.7.2.3. Arrangements for limited projection topographs and direct-beam topographs.

In certain investigations, the methods of $\mathbf{K}_h$-beam 'limited projection topographs' (Lang, 1963) and of $\mathbf{K}_0$-beam section topographs and projection topographs are useful; Fig. 2.7.2.3 shows the arrangement of screens and diffracted-beam slits then adopted. The limited projection topograph technique can be employed with a plate-shaped specimen $CDD'C'$, as in the following examples. Suppose the surface of the plate contains abrasion damage that cannot be removed but that causes diffraction contrast obscuring the images of interior defects in the crystal. The diffracted-beam slit (equivalent to the opening in $Q$ shown in Fig. 2.7.2.2), which is opened to the setting $S_1$ for a standard projection topograph, may now be closed down to setting $S_2$ so as to cut into the $RR'$ and $TT'$ edges of the $\mathbf{K}_h$ beam, and thereby prevent direct images of near-surface defects located between $CC'$ and $XX'$, and between $YY'$ and $DD'$, from reaching $F$. As another example, it may be desired to receive direct images from a specimen surface and a limited depth below it only (*e.g.* when correlating surface etch pits with dislocation outcrops). Then, setting $S_3$ of the diffracted-beam slit is adopted and only the direct images from defects lying between depth $ZZ'$ and the surface $DD'$ reach $F$.

To record the $\mathbf{K}_0$ beam image, either in a section topograph or a projection topograph, some interception of the $\mathbf{K}_0$ beam on the $OTT''$ side is needed to avoid intense blackening of the film $G$ by radiation coming from the source, which will generally contain much energy in wavelengths other than those undergoing Bragg diffraction by the crystal. Screen $S_4$, critically adjusted, performs the required interception. Recording both $\mathbf{K}_0$-beam and $\mathbf{K}_h$-beam images is valuable in some studies of dynamical diffraction phenomena, such as the 'first-fringe contrast' in stacking-fault fringe patterns (Jiang & Lang, 1983). Such recording can be done simultaneously, on separate films, normal to $\mathbf{K}_0$ and $\mathbf{K}_h$, respectively, when $2\theta_B$ is sufficiently large.

When collimated characteristic radiation is used, recording projection topographs of reasonably uniform density becomes difficult when the specimen is bent. To keep the $\omega$ axis oriented at the peak of the Bragg reflection while the specimen is scanned, several devices for 'Bragg-angle control' have been designed, for example the servo system of Van Mellaert & Schwuttke (1972). The signal is taken from a detector registering the Bragg reflection through the film $F$, but this precludes use of glass-backed emulsions if X-ray wavelengths such as that of Cu $K$ and softer are used. An alternative approach with thin, large-area transmission specimens is to revert to the geometry of Fig. 2.7.1.2 and deliberately elastically bend the crystal to such radius as will enable its whole length to Bragg diffract a single wavelength diverging from $S$, similar to a Cauchois focusing transmission monochromator (Wallace & Ward, 1975). No specimen traversing is then needed, but $b$ cannot be made small if the wide $\mathbf{K}_0$ and $\mathbf{K}_h$ beams are to be spatially separated in the plane of $F$.

Quite simple experimental arrangements can be adopted for taking transmission topographs under high-absorption conditions, when only anomalously transmitted radiation can pass through the crystal. The technique has mainly been used in symmetrical transmission, as shown with the specimen $CC'D'D$ in Fig. 2.7.2.4. When the specimen perfection is sufficiently high for the Borrmann effect to be strongly manifested, and $\mu t > 10$, say, the energy flow transmitted within the Borrmann triangle is constricted to a narrow fan parallel to the Bragg planes, the fan opening angle being only a small fraction of $2\theta_B$ [see *IT* B (1996, Part 5)]. Radiation of a given wavelength coming from a small source at $S$ and undergoing Bragg

diffraction in $CC'D'D$ will take the path shown by the heavy line in Fig. 2.7.2.4, simplifying the picture to the case of extreme confinement of energy flow to parallelism with the Bragg planes. At the X-ray exit surface $DD'$, splitting into $\mathbf{K}_0$ and $\mathbf{K}_h$ beams occurs. A slit-less arrangement, as shown in the figure, may suffice. Then, when $S$ is a point-like source of $K\alpha$ radiation, and distance $a$ is sufficiently large, films $F_1$ and $F_2$ will each record a pair of narrow images formed by the $\alpha_1$ and $\alpha_2$ wavelengths, respectively. A wider area of specimen can be imaged if a line focus rather than a point focus is placed at $S$ (Barth & Hosemann, 1958), but then the $\alpha_1$ and $\alpha_2$ images will overlap. Under conditions of high anomalous transmission, defects in the crystal cause a reduction in transmitted intensity, which appears similarly in the $\mathbf{K}_0$ and $\mathbf{K}_h$ images. Thus, it is possible to gain intensity and improve resolution by recording both images superimposed on a film $F_3$ placed in close proximity to the X-ray exit face $DD'$ (Gerold & Meier, 1959).

### 2.7.3. Double-crystal topography

The foregoing description of single-crystal techniques will have indicated that in order to gain greater sensitivity in orientation contrast there are required incident beams with closer collimation, and limitation of dispersion due to wavelength spread of the characteristic X-ray lines used. It suggests turning to prior reflection of the incident beam by a perfect crystal as a means of meeting these needs. Moreover, the application of crystal-reflection-collimated radiation to probe angularly step by step as well as spatially point by point the intensity of Bragg reflection from the vicinity of an individual lattice defect such as a dislocation brings possibilities of new measurements beyond the scope provided by simply recording the local value of the integrated reflection. The X-ray optical principles of double-crystal X-ray topography are basically those of the double-crystal spectrometer (Compton & Allison, 1935). The properties of successive Bragg reflection by two or more crystals can be effectively displayed by a Du Mond diagram (Du Mond 1937), and such will now be applied to show how collimation and monochromatization result from successive reflection by two crystals, $U$ and $V$, arranged as sketched in Fig. 2.7.3.1. They are in the dispersive, antiparallel, '$++$' setting, and are assumed to be identical perfect crystals set for the same symmetrical Bragg reflection. Only rays making the same glancing angle with both surfaces will be reflected by both $U$ and $V$. For example, radiation of shorter wavelength reflected at a smaller glancing angle at $U$ (the ray shown by the dashed line) will impinge at a larger glancing angle on $V$ and not satisfy the Bragg condition. In this $++$ setting, with a given angle $\omega$ between the Bragg-reflecting planes of each crystal, $\theta_U + \theta_V = \omega$ and $\Delta\theta_U = -\Delta\theta_V$. The Du Mond diagram for the $++$ setting, Fig. 2.7.3.2, shows plots of Bragg's law for each crystal, the $V$ curve being a reflection of the $U$ curve in a vertical mirror line and differing by $\omega$ from the $U$ curve in its coordinate of intersection with the axis of abscissa, in accord with the equations given above. The small angular range of reflection of a monochromatic ray by each perfect crystal is represented exaggeratedly by the band between the parallel curves. Where the band for crystal $U$ superimposes on the band for $V$ (the shaded area) defines semiquantitatively the divergence and wavelength spread in the rays successively reflected by $U$ and $V$. (It is taken for granted that $\frac{1}{2}\omega$ lies between the maximum and minimum incident glancing angles on $U$, $\theta_{\max}$ and $\theta_{\min}$, afforded by the incident beam, assumed polychromatic.) The reflected beam from $U$ alone contains wavelengths ranging from $\lambda_{\min}$ to $\lambda_{\max}$. Comparison of these $\theta$ and $\lambda$ ranges with the extent of the shaded area illustrates the efficacy of the $++$ arrangement in providing a collimated and monochromatic beam, which can be employed to probe the reflecting properties of a third crystal (Nakayama, Hashizume, Miyoshi, Kikuta & Kohra, 1973). Techniques employing three or more successive Bragg reflections find considerable application when used with synchrotron X-ray sources, and will be considered below, in Section 2.7.4.

The most commonly used arrangement for double-crystal topography is shown in Fig. 2.7.3.3, in which $U$ is the 'reference' crystal, assumed perfect, and $V$ is the specimen crystal under examination. Crystals $U$ and $V$ are in the parallel, '$+-$' setting, which is non-dispersive when the Bragg planes of $U$ and $V$ have the same (or closely similar) spacings. Before considering the Du Mond diagram for this arrangement, note that Bragg reflection at the reference crystal $U$ is asymmetric, from planes inclined at angle $\alpha$ to its surface. Asymmetric reflections have useful properties, discussed, for example, by Renninger (1961), Kohra (1972), Kuriyama & Boettinger (1976), and Boettinger, Burdette & Kuriyama (1979). The asymmetry factor, $b$, of magnitude $|\mathbf{K}_0 \cdot \mathbf{n}/\mathbf{K}_h \cdot \mathbf{n}|$, $\mathbf{n}$ being the

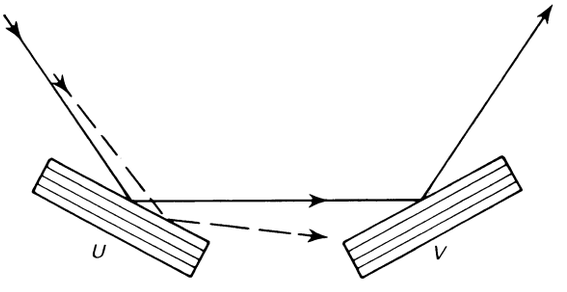


Fig. 2.7.3.1. Double-crystal $++$ setting.

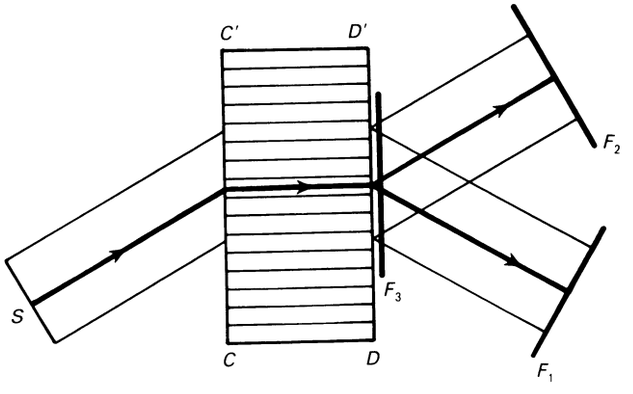


Fig. 2.7.2.4. Topographic techniques using anomalous transmission.

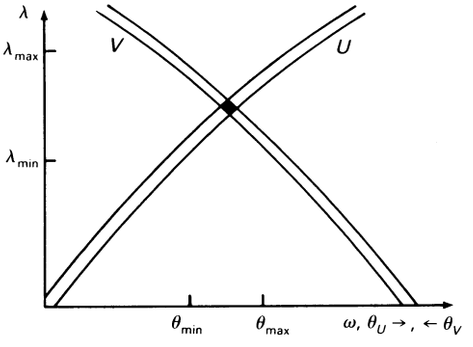


Fig. 2.7.3.2. Du Mond diagram for $++$ setting in Fig. 2.7.3.1.



references